Aluminium Filtration by Bonded Particle Filters

Anne Kvithyld[1], Martin Syvertsen[1], Sarina Bao[1], Ulrik Aalborg Eriksen[1],
Inge Johansen[2], Eilif Gundersen[2], Shahid Akhtar[2],
Terje Haugen[3] and Britt Elin Gihleengen[3]

[1]SINTEF Industry, Trondheim, Norway

[2]Hydro Aluminium, Sunndal, Norway

[3]Hycast, Sunndal, Norway

Corresponding author: *Anne Kvithyld*, Alfred Getz vei 2, NO-7034 Trondheim, Norway

e-mail: Anne.Kvithyld@sintef.no

Abstract

Non-metallic inclusions such as oxides, borides and carbides in aluminium melts are a major cause of product failure during both processing and use. To remove these inclusions, molten aluminium is usually filtered through a mechanical filter such as deep bed-filter, ceramic foam filter or Bonded Particle Filter (BPF).

In this study three BPF from Pyrotek have been tested at Hydro's reference centre in Sunndalsøra. The filters had different grit sizes; 6, 10, and 14 (equivalent to 30, 50, and 70 ppi). The filters were mounted in the patent pending Drain Free filter box developed by Hycast. LiMCA was used at the up-stream side of the two coarsest filter (Grit 6 and 10) and both up-stream and down-stream for the finest filter (Grit 14). Three samples from each of the filters have been studied in a light microscope, and inclusions have been counted using image analysis. In addition, PoDFA samples from the test with the finest filter were also analysed and discussed.

Introduction

Refining by filtration of molten metal is increasingly important. Non-metallic inclusions are removed in deep bed-, ceramic foam-, or bonded particles filters.

There are many theories on filtration. Mechanisms are often split into two or three; cake-, depth-, and alternatively also sieve mode. However, even though filtration of aluminium has been practiced for more than 40 years [1] there are still many questions regarding the mechanism. One reason for this is the high number of parameters affecting the filtration efficiency. Bao summarized effects affecting the filtration efficiency in her PhD-thesis [2] into:

- *Inclusions parameters* such as composition, specific gravity, size and number.
- *Filter parameters* such as filter type, filter materials, depth of the filter media, pore size, location in the runner and mechanical filter strength (hot and cold).
- *Process parameters* such as Reynolds number, residence time, filtration time, the size of filter characteristics (geometry), gravitational number, presence of grain refiners, and preheating and priming of the filters.

The aim of the paper is to describe the filtration efficiency of a bonded particle filter and indirectly look at some of the filtration parameters. According to Pyrotek, Bonded Particle Filters (BPF) operate in both the cake and depth filtration modes for inclusion capture. Figure 1, provided by the producer, shows the conversion between the BPF grit sizes and ppi used for CFF. This shows that 6 – 12 grit corresponds to 30 – 70 ppi.

Bonded Particle Filter (BPF) grit	Ceramic Foam Filter (CFF) grade
6	30–39 ppi
8	40–49 ppi
10	50–59 ppi
12	60–69 ppi

Figure 1: Picture from [3] on the relation between ppi number for CFF and grit number for BPF.

Experimental

Alloys

Filters of size 23 inch square of grit sizes 6, 10 and 14 were tested at the reference centre of Hydro at Sunndalsøra in Norway. When received, the filters were equipped with standard, non-expanding gaskets. After the first trials it was decided to replace the gasket on the grit 14 filter with an expanding gasket. The metal was received from a dross remelter and contained about 97 % aluminium. The metal used in the tests was therefore not in accordance with standard alloys. This gave some challenges in the PoDFA sample analysis. Table 1 shows some of the alloying elements. A complete list of alloying elements is in reference [4].

Table 1: Spectrographic analyses of the metal in the three experiments

	Grit 6 experiment	Grit 10 experiment	Grit 14 experiment
Al	97.8	96.6	96.8
Si	0.73	2.5	0.83
Fe	0.17	0.40	0.30
Cu	0.16	0.11	0.84
Mn	0.35	0.31	0.51
Mg	0.51	0.04	0.61

The Experimental Setup and Process Parameters

Figure 2 shows a schematic of the experimental setup with the furnace, launder system, filter box, and metal pump. Also indicated are the positions of the LiMCA and PoDFA sampling, and the lasers which are used to measure the pressure drop over the filter during filtration. The melt flow is indicated with the arrows inside the launder. In the bottom of the furnace there are two porous plugs with a total capacity of 120 Nl/min of argon gas. These plugs were run for ten minutes during the tests to increase the inclusion content in the launder.
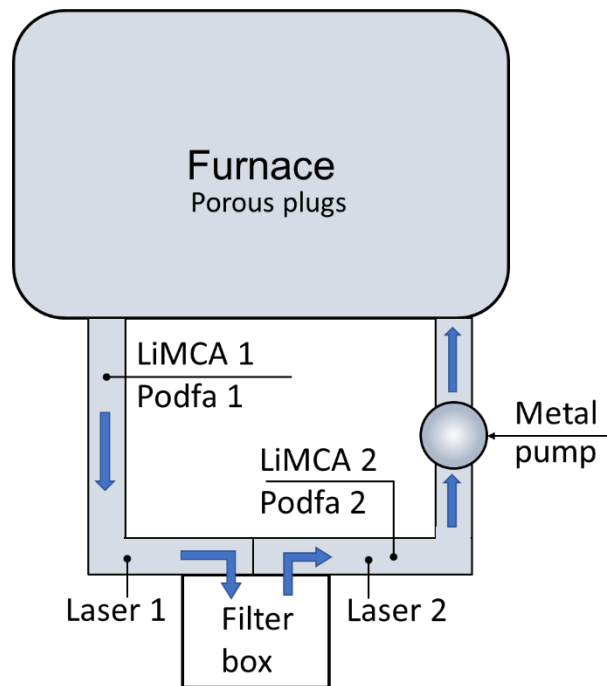

Figure 2: Schematic of the loop system at the research centre at Hydro Sunndalsøra. The furnace has a capacity of 20 tons. The positions of the various measurement instruments are indicated by the black connectors and melt flow direction by the blue arrows

The filters were put into the patented filter box [5], and preheated by a 30 kW hot air blower set to maximum 800 °C. In this box the metal is lifted by vacuum so that the filter is primed from below. After the filter is primed, the metal is lifted further up and above the internal dam. Then the metal flow is reversed so that the metal flows down through the filter during normal operation. The filter box lid is equipped with a window enabling observation of the filter priming. The priming height is defined as the height difference between the top of the filter, when the melt has come through the filter, and the melt level on the other side of the dam.

In Table 2 a summary is given of the process parameters for the three filtrations experiments, which are discussed further in the paper.

Table 2: Process parameters during the priming and filtration tests

Filter	Grit 6	Grit 10	Grit 14
Temperature filter before priming	631 °C	579 °C	632 °C

Melt temperature up-stream the filter	747 °C	748 °C	746 °C
Melt temperature down-stream the filter	718 °C	732 °C	723 °C
Priming height	150 mm	260 mm	330 mm
Average hydrogen	0.18 ml/100g	0.14 ml/100g	0.26 ml/100g
Typical LiMCA N20 Values Up-stream filter	10 k/kg	2,2 k/kg	66 k/kg
Metal flow	11 t/h	16 t/h	11 t/h
Plugs used	10 min	10 min	10 min
Metal in the filter	7.6 kg	6.9	7.5
PoDFA samples	No	Not available	Yes

Image Analysis

The inclusions captured in the filter were studied under light microscope, with an emphasis on looking at the variance in performance between the different grit sizes. A complete description of the sample preparation and image analysis is given in the report by Eriksen [4].

Figure 3 shows the position of the three samples taken from each filter; one at the edge, one in the centre, and one between them. The samples were roughly a cube with sides of 25 mm. In Figure 4 images of each filter grit filled with metal are shown. The pictures are taken with the same resolution emphasising the difference in packed bonded particles sizes.
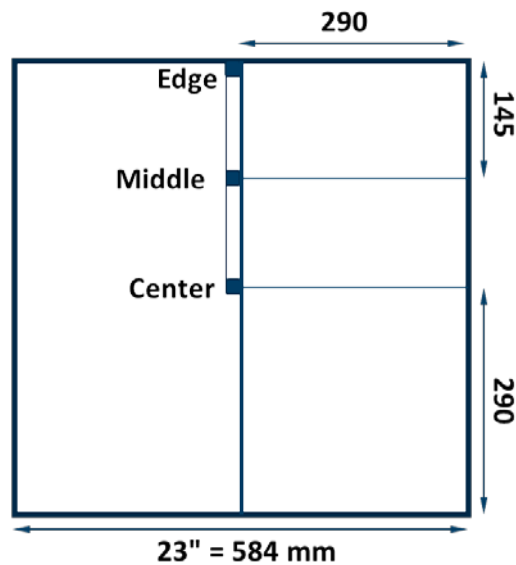

Figure 3: Position of filter samples in the filter seen from above. Cylindrical symmetry is assumed so that the samples are representative for most of the filter area

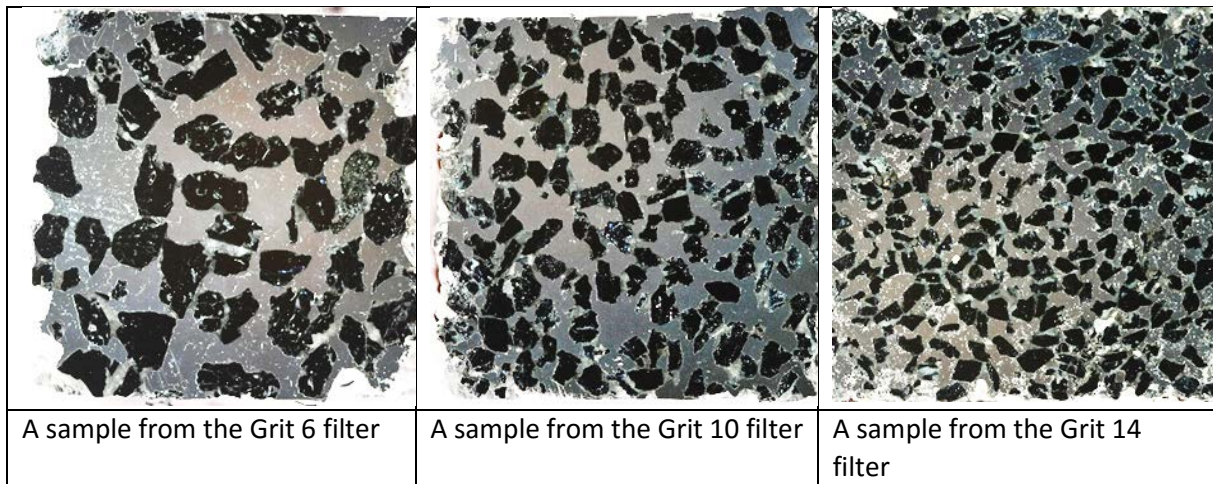| A sample from the Grit 6 filter | A sample from the Grit 10 filter | A sample from the Grit 14 filter |

Figure 4: Pictures of three filter samples. One from each grit illustrating the filter particle size and porosity. The pictures show the total filter height of 25 mm

A challenge with image analysis of such filter samples is to distinguish between inclusions, intermetallics, BPF-particles, and polishing marks. Evaluation is based on size, shape, colour and localization. Examples of what is included in the counting and what is excluded are shown in Figure 5. A full description together with a prediction of which phases are formed is found in the cited report [4].

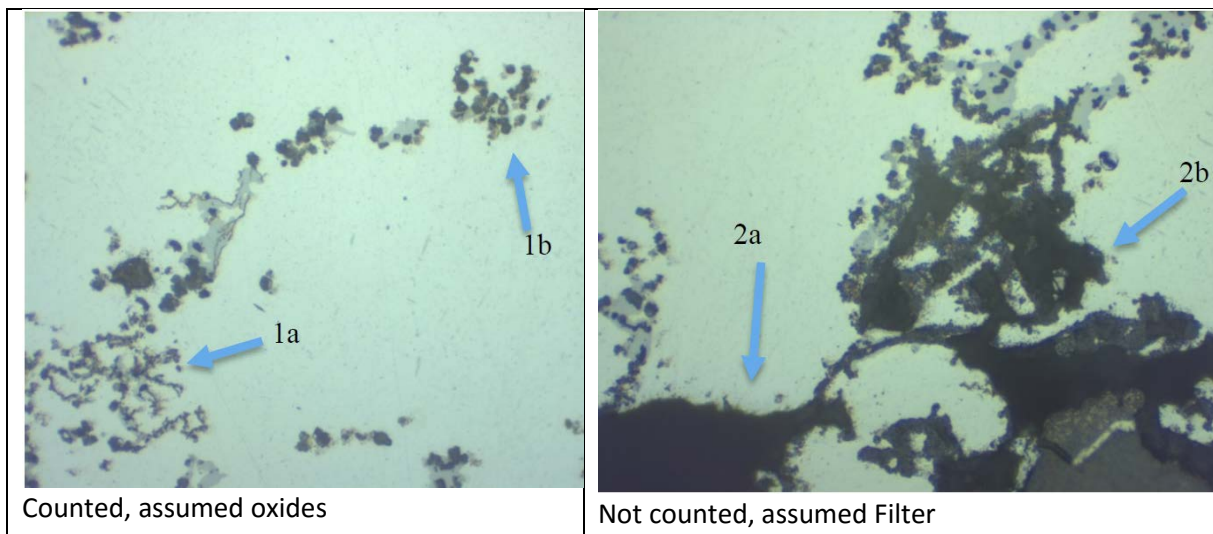| Counted, assumed oxides | Not counted, assumed Filter |

Figure 5: Two micrographs of a filter sample showing oxide particles at the left hand picture and parts of filter media on the right hand picture, indicated by blue arrows. The micrographs cover an area of about $200 \times 150 \ \mu m^2$

All pictures were taken with a magnification of 50 times and at a resolution of 2080×1542 pixles^2. They were analysed using the ImageJ software.

Picture series of 11 pictures with 0.2 mm spacing, which were taken and analysed, covering about 10 % of the cross section. To get more reliable results, a minimum of 25 % aluminium matrix is required to be included in the picture. Low matrix percentages will give too high inclusion fraction readings. To get rid of noise picked up by the software, a minimum diameter of 1 µm was set as a lower limit for inclusions.

Results and Discussion

Priming

Figure 6 shows two pictures of the filter priming taken through the window in the filter box lid. The pictures show a top-down view of the filters during priming, as metal has penetrated the filter. For the Grit 6 filter, there are small metal droplets on the filter surface, which means the priming was good. For Grit 10 the metal is running across the filter indicating a metal flow between the filter and filter box. This is probably due to the not expanding gaskets. For Grit 14, where we had replaced the gasket with an expanding one, the visual inspection indicated metal penetration from below. That is the priming of Grit 14 seemed to be good.

Grit 6 | Grit 10

Figure 6: Priming of the filters taken through the glass showing good and bad priming of grit 6 and 10, respectively.

Figure 7 shows the measured pressure drop over the filters as a function of time. The pressure drop is calculated from the difference between the two melt heights measured by laser 1 up-stream, and laser 2 down-stream of the filter. Time zero is when the metal was observed to have penetrated through the filter (as indicated in Figure 6 for Grit 6). The pressure drop over the filters likely stabilised; for Grit 14 at 55 mm, Grit 10 at 25 mm, and Grit 6 at 5 mm. The time before stabilisation is around an hour for Grit 10 and 14 whereas Grit 6 is stable after approximately 15 minutes. However, the development of the pressure drops is very different in the 3 cases. The densest filter, Grit 14, is increasing in pressure drop with time, indicating that the resistance in the filter is increasing. Grit 10 has a decrease in pressure drop with time. This is assumed to be caused by the poor priming of the filter. Possible explanations are that either more of the filter is available for metal flow, or that an increased fraction of metal flows past the filter, between the filter and filter box, after some time. A constant pressure drop means that the resistance in the filter is not changing.
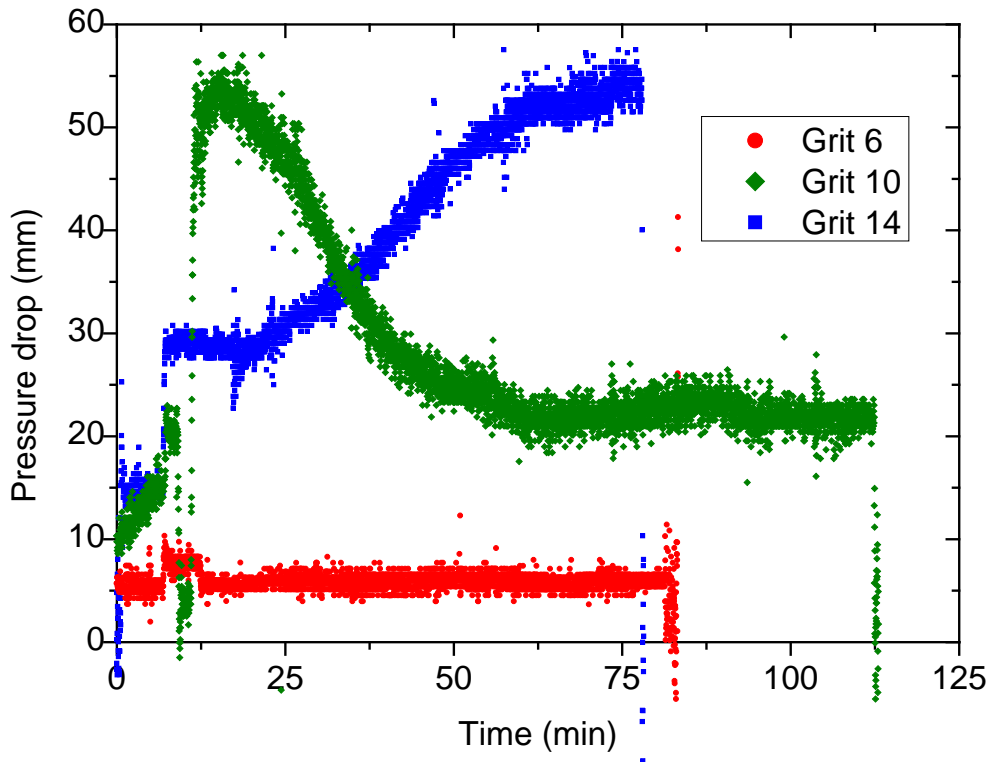
Figure 7: Measured pressure drop over the filter from start until the end of the experiments for all three grits

LiMCA and PoDFA for Grit 14

Below are the N20 LiMCA data for Grit 14 up- and down-stream the filter shown. Note the different scales on the up-stream and down-stream vertical axes. To increase the inclusion content in the metal, gas purging in the furnace was done between 36 and 46 minutes from the start as indicated on the graphs. This gave large peaks in the measured inclusion content both up-stream and down-stream the filter. The time lag between the peaks in the N20 data is taken as the time for the metal to travel from LiMCA number 1, through the filter box, and to LiMCA number 2. The rightmost figure shows the data when the N20 data have been shifted.
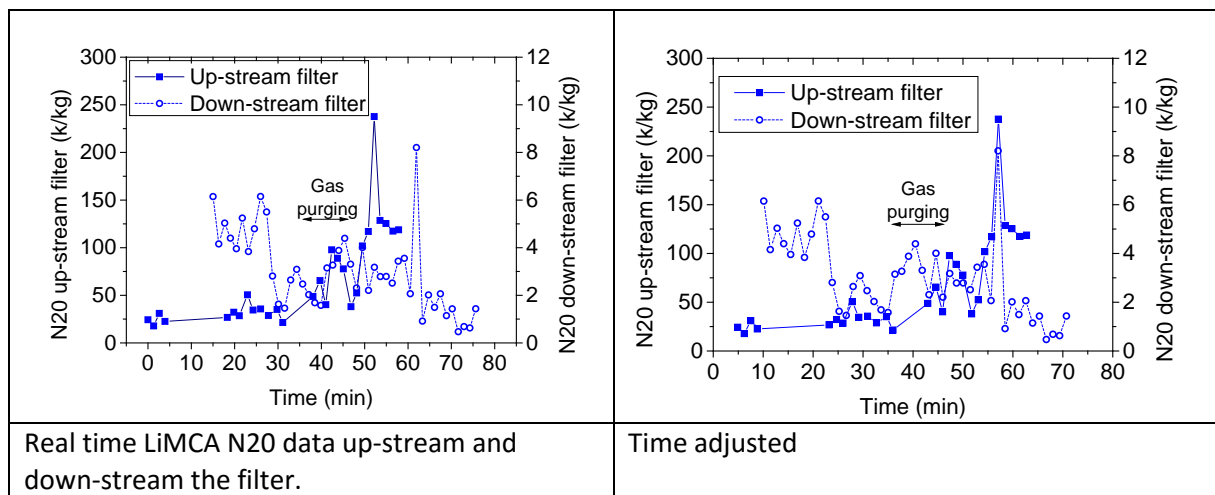

| Real time LiMCA N20 data up-stream and down-stream the filter. | Time adjusted |

Figure 8: N20 LiMCA data up- and down-stream for the Grit 14 filter.

In order to calculate the removal efficiency in the filter, the time shifted N20 data are used. In addition, since the LiMCA-data are not evenly distributed, interpolation of the N20 measurements up-stream the filter onto the time for the N20 measurements down-stream the filter has also been done. As usual, the removal efficiency in the filter is defined as:

$$E = \left(1 - \frac{N20_{Down-stream}}{N20_{Up-stream}}\right) \cdot 100\%$$

Based on the picture to the right in Figure 8, the removal efficiency is calculated. The removal efficiency is shown in Figure 9 as black stars, with the up- and down-stream N20 values in blue. The removal efficiency is mainly in the range of 70 – 99 %.
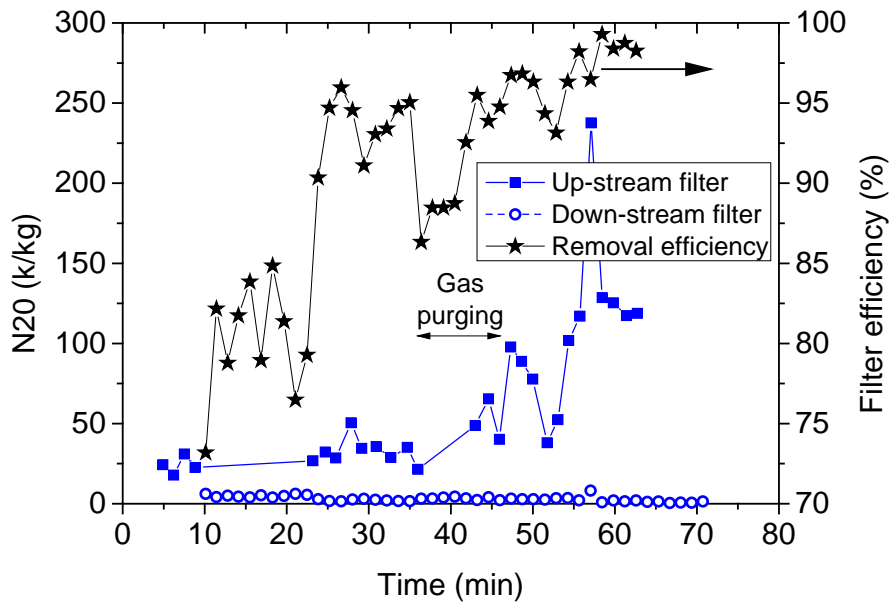

Figure 9: Time shifted LiMCA N20 measurements up- and down-stream filter together with calculated removal efficiency as function of time. In addition to the time shift, the N20 values up-stream filter is interpolated to the time when the N20 down-stream filter are measured and used in the efficiency calculations

Below in Table 3 are the PoDFA values up- and down-stream the filter for the Grit 14 experiment, and before and after gas purging. The calculated removal efficiencies are similar to the filtration efficiency calculated from the LiMCA data.

Unfortunately, the PoDFA vacuum system was not working properly for the grit 6 experiment, and for the Grit 10 experiment, the PoDFA samples should be re-examined in order to establish reliable numbers.

Table 3: PoDFA values from the Grit 14 experiment with calculated filtration efficiencies

	Oxides up-stream filter (mm²/kg)	Oxides down-stream filter (mm²/kg)	Removal efficiency of oxides (%)
Grit 14 before purging	0.112	0.031	72
Grit 14 after purging	0.101	0.011	89

One must be careful not to put too much confidence into comparing the PoDFA and LiMCA results since they generally are measuring different sizes of inclusions. The PoDFA samples include inclusions

down to about 1 µm, while (according to ABB) LiMCA measurements below 20 µm should be considered unreliable.

Data from Image Analysis of the Samples from the Three Different Grits

The recorded inclusion- and filter areas are used to calculate the inclusion percentage for all the samples. These percentages are shown in Figure 10 as function of filter depth. From the figure is seen that the highest inclusion concentrations are found in the finer grits and at the inlet, as expected. There also seems to be a tendency for inclusion concentration to be highest at the edge of the filter, and lowest in the centre.
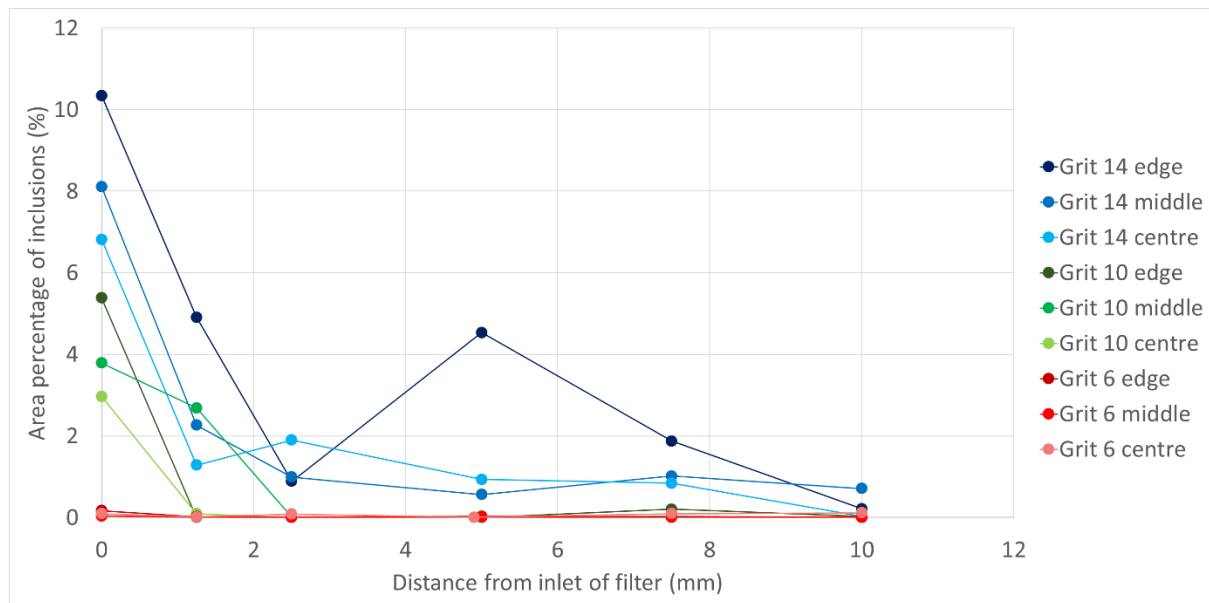

Figure 10: A summary of all inclusion percentages for all samples at depths ranging from 0 to 10 mm from the inlet of the filter

It should be noted that the inclusion concentration is not homogenous across the cross sections, instead the concentration appears to be heavily affected by the filter geometry with inclusions forming clusters at locations with back currents. This results in large differences in inclusion concentration within the same picture series at a given depth. From the results it is evident that Grit 14 captures a lot more of the small inclusions than the coarser grits. However, this difference in number of captured inclusions decreases with increasing inclusion size. See the calculated inclusion densities in Figure 11. These are calculated according to:

$$Density = \frac{Number\ of\ particles\ in\ the\ given\ size\ range}{Area\ of\ aluminium\ matrix}$$

Note the scale on the y-axis is logarithmic.

The density for inclusions with size range $1 - 10$ µm is in the order of $10\ 000$ mm^{-2} whereas the inclusions with size range $10 - 20$ µm are in the order of 100 mm^{-2}. It is also worth noting the density difference within the group of $1 - 10$ µm. Grit 10 and 6 seems to capture the small inclusion with the same efficiency (density order of $1\ 000$ mm^{-2}) whereas Grit 14 is much more efficient (density is in the order of $10\ 000$ mm^{-2}). This means that Grit 14 is much more efficient than Grit 10 and 6 for the small inclusions.
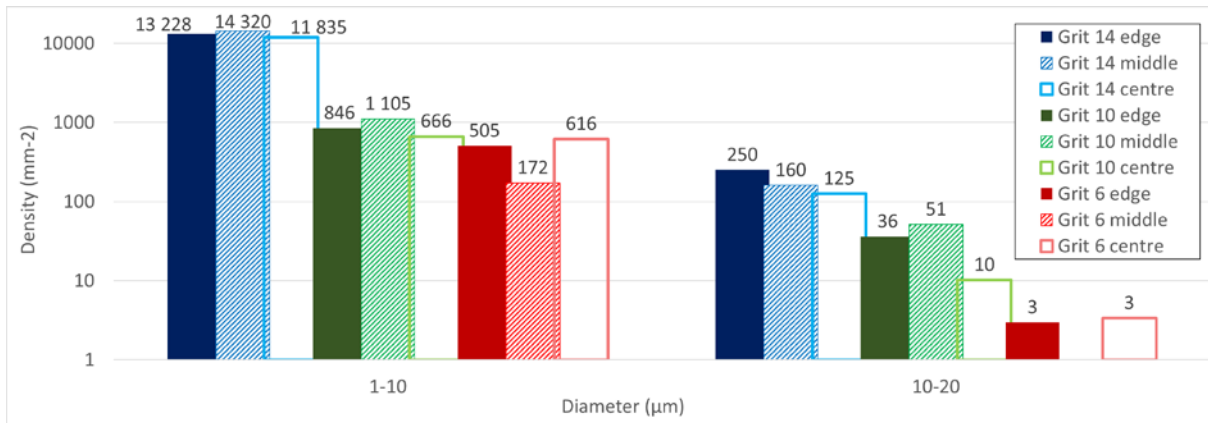
Figure 11: Inclusions per square millimetre metal matrix in the filter versus inclusion diameter, comparison between size ranges 1 – 10 µm and 10 – 20 µm

Figure 12 shows the pressure drop and removal efficiency of Grit 14. The values seem to correlate. When inclusions are captured in the filter the pressure drop increases, possibly due to build-up of an inclusion layer in the filter and hence increased flow resistance.
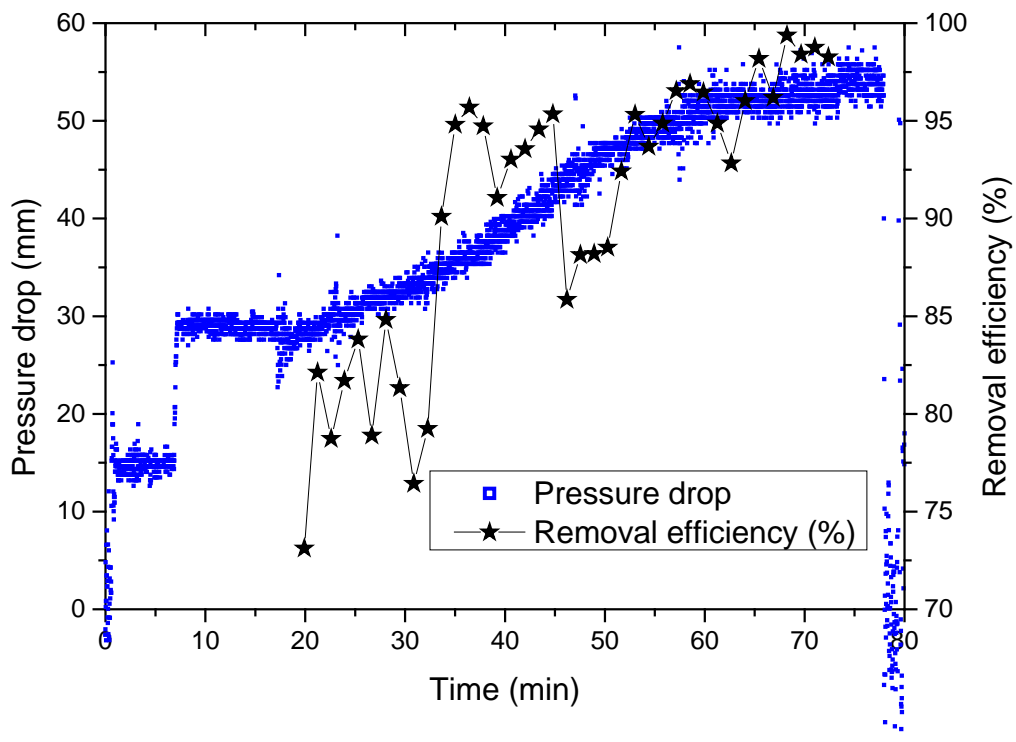

Figure 12: Pressure drop and removal efficiency for the Grit 14 filter experiment

The results from counting the inclusions in the filter show that Grit 14 is by far the most efficient. Also, from the image analysis it seems that most inclusions are captured within the first 10 mm of the filter.

The LiMCA measurements with Grit 14 gave a high removal efficiency ranging from about 80 % to more than 95 %. It is worth noting the filtration times of 1 – 1.5 hours. It will be important to study longer times.

Comparing with other studies is difficult due to as mentioned in the introduction the high number of parameters affecting the filtration efficiency. Lae et.al. [6] summarized different standard CFF and showed the wide range of CFF efficiencies from 30 – 60 % to 80 – 90 %. The same group, (Duval et. al. [7]) also counted the number of inclusions "post mortem" in a 30 ppi CFF filters as a function of the depth and found that the first two millimetres from the inlet had inclusion per unit volume of around 8000 cm^{-3} compared to less than 2000 cm^{-3} further into the filter. In the paper by Le Roy [8] efficiency numbers based on both LiMCA N20 and PoDFA analysis is presented for BPF with high 90'es based on LiMCA readings. For PoDFA, a slight downwards trend is shown from 100% to 90% over the period of filtration 4000 tonnes of metal. Syvertsen [9] published in his thesis LiMCA data showing removal efficiencies of generally more than 97 % for inclusions larger than 20 µm. Hence, measured removal efficiency in the BPF is closer to the removal efficiency in deep bed filters.

Conclusion

The performance of three different BPF have been tested.

- The results show that it is possible to prime the bonded particle filter in the filter box.
- The removal efficiency for Grit 14 is in the range 80 % to more than 95 %.
- Most inclusions are captured in the first 10 mm of the filter.

Future work

Unfortunately, there are too many variables in the experiments, e.g. gaskets, too few LiMCA readings, non-standard alloys, and last but not least various inlet concentrations K/kg. Further experiments minimising these errors are necessary. In addition, it will be important to study longer filtration times.

References

1. J.E. Dore and J.C. Yarwood: *Ceramic foam - A unique method of filtering molten aluminium alloys*, Light Metals 1977, pp. 171 – 189
2. S. Bao: *Filtration of Aluminium – Experiments, Wetting, and Modelling*, PhD-thesis NTNU 2011:301, pp. 39 – 49
3. Pyrotek, 824 Bonded Particle Filters, https://www.pyrotek.com/DeliverFile/a7d2ca59d9a51fee524673375ec137da
4. U. Aalborg Eriksen: *Inclusion counting in BPF-Filters*, SINTEF report 2018:00957 - Unrestricted
5. U. Tundal and I.K. Steen: *Apparatus and method for removal of unwanted inclusions from metal melts*, WO2016126165A1 – P15002
6. E. Lae, et. al: *Experimental and Numerical Study of Ceramic Foam Filtration*, Light Metals 2006, pp: 753 – 758
7. H. Duval, et. al: *Simulation of Aluminum Filtration Including Lubrication Effect in Three-Dimensional Foam Microstructures*, Light Metals 2007, pp. 645 – 650
8. G. Le Roy, J-M. Chateau, and P. Charlier: *PDBF: Proven Filtration for High-End Applications*, Light Metals 2007, pp. 651 – 655
9. M. Syvertsen: *Removal of Hydrogen and Inclusions from Aluminium*, Dr.ing.-Thesis NTNU 2000:50